IJCFD, 2000, Vol. 00, pp. 1 - 17
Reprints available directly from the publisher
Photocopying permitted by license only

Computation of Internal and External Compressible Flows Using *EDICT*

SANJAY MITTAL*

Department of Aerospace Engineering, Indian Institute of Technology, Kanpur, UP 208 016, India

(Received 20 May 2000; In final form 26 October 2000)

Results are presented for finite element computations involving high speed, viscous compressible internal and external flows. The stabilized finite-element formulations for the Navier-Stokes equations in the conservation law form are solved using the conservation variables. To improve the accuracy of the base method, especially in the regions of flow that are associated with shocks, boundary-layers and their interactions, the Enhanced-Discretization Interface-Capturing Technique (*EDICT*) is utilized. An error indicator is employed to identify the regions in the computational domain that need enhanced discretization for increased accuracy. The method is implemented on a shared-memory parallel computer and is used to study complex flows, that involve shock-wave/boundary-layer interactions, in supersonic diffusers and wind-tunnels. The *start-up* problem in supersonic wind-tunnels, caused by a narrow *second throat* in the diffuser section, is simulated. This computation brings out some of the very interesting features of the unsteady dynamics of the start-up shock.

Keywords: supersonic diffusers, wind-tunnels, EDICT, viscous flows

INTRODUCTION

In this article, results are presented for finite element computation of internal and external supersonic flows. Most of the computations are carried out using the Enhanced-Discretization Interface-Capturing Technique (*EDICT*) that was introduced by Tezduyar *et al.* [1, 2] for simulation of unsteady flow problems with interfaces such as two-fluid and free-surface flows. Later Mittal *et al.* [3] demonstrated, through certain examples, the application of *EDICT* to unsteady compressible flow problems. This technique is useful in accurate computation of unsteady flows that involve shock/boundary-layer interactions. Internal flows in supersonic wind-tunnels, especially in the diffuser section, involve such complex interactions. Internal flows have been investigated by several researchers in the past. A review of the data-base available for shock-wave/boundary-layer interactions in supersonic inlet has been presented by Hamed and Shang [4]. Polsky and Cambier [5]

*e-mail: smittal@iitk.ac.in

studied the transient flow through a shock tunnel using Euler equations. Chen, Chakravarthy and Hung [6] used the Reynolds-averaged Navier-Stokes equations to study separated flow through converging-diverging nozzles and Argrow and Emanuel [7] investigated the transonic flow field in a 2D minimum length nozzle. Causon *et al.* [8] have applied their high resolution shock capturing methods, using Euler equations, to study surge in aircraft engine intakes. Reddy and Weir [9] have simulated three-dimensional flow in a $Mach = 5$ inlet and compared it with experimental results. It appears that there have been a number of successful studies with the Euler equations, however, there have been relatively fewer efforts to address the complex details of the shock/boundary-layer interactions in internal flows.

The governing equations for the flow are the compressible Navier-Stokes equations in the conservation law form. They are solved using a stabilized finite element formulation based on conservation variables. The SUPG (streamline-upwind/Petrov-Galerkin) stabilization technique is employed to stabilize the computations against spurious numerical oscillations due to advection dominated flows. A shock-capturing term is added to the formulation to provide stability to the computations in the presence of discontinuities and large gradient in the flow. Many of the computations reported in this article are carried out using *EDICT* [1, 3]. An error indicator, proposed by Lohner [10], is employed to identify the regions in the computational domain that need enhanced discretization for increased accuracy. Usually, these regions are the ones that are associated with large gradients of the flow variables. The finite element functions corresponding to enhanced discretization are designed to have two components, with each component coming from a different level of mesh refinement over the same computational domain.

Results are presented for, both, internal and external high-speed flow. Supersonic flow past a circular cylinder is solved using the *EDICT* to demonstrate its effectiveness in resolving sharp gradients in external flows. The application of the base finite-element formulation to various flow problems involving external flow past cylinders and airfoils in various speed regimes has been reported in earlier articles [11, 12]. In this article the main emphasis is on the computation of internal flows. First, the method is checked against a couple of benchmark problems. The first one is a flow in a double throat nozzle. Results for this problem have been computed by other researchers and reported in a *GAMM workshop* [13]. An important feature of the flows in the supersonic diffusers is the interaction of shocks and boundary layers. To validate the present formulation for such flows the second benchmark problem is the *Mach* 3 flow past a 10° compression corner. The results compare quite well with those reported by Shakib [14], Carter [15] and Hung and MacCormack [16]. Next, flow in the diffuser section of a supersonic wind-tunnel is investigated. The supersonic diffuser, located just downstream of the test-section, is responsible for slowing the flow and recovery of static pressure *via* a train of oblique shocks and viscous action. *EDICT* is employed to resolve the complex interactions involving shocks and boundary layers. In one of the simulations, the *start-up* problem of a supersonic wind-tunnel is investigated. It is well known that for a fixed geometry diffuser the area of the constant area section must not be less than that required to *start* the flow. Otherwise, an unsteady shock-wave, such as the one obtained during start-up, is not swallowed by the diffuser and the tunnel may *unstart*. A fully developed *Mach* 5 flow is specified at the inlet of the test-section of a wind-tunnel, whose diffuser has a constant-area section that is too narrow to allow the start-up shock to pass through. The computations are able to predict the *unstarting* of the tunnel and contribute to the understanding of the underlying mechanism. This is, perhaps, the first attempt to simulate this complex phenomenon. Finally, the flow through an entire wind-tunnel with a wedge nozzle block is simulated. This is a time-accurate computation and is capable of predicting the start-up effects. A

useful tool has been developed that may be utilized for the design of diffuser sections of wind-tunnels or aircraft engine intakes.

The equation systems resulting from the finite element discretization of the flow problems are solved iteratively using a matrix-free technique to reduce the memory requirements. This vector-based technique [17] eliminates the need to compute or store any coefficient matrices including those at the element level. The method has been implemented on a shared-memory parallel multiprocessor computer from *SGI*.

In Section 2 the governing equations for compressible fluid flow are reviewed. The stabilized formulations along with the description for enhanced discretization are described in Section 3. Results and discussion constitute Section 4 and a few concluding remarks are made in Section 5.

2. THE GOVERNING EQUATIONS

Let $\Omega \subset \mathbb{R}^{n_{sd}}$ and $(0, T)$ be the spatial and temporal domains respectively, where n_{sd} is the number of space dimensions, and let Γ denote the boundary of Ω. The spatial and temporal coordinates are denoted by $\mathbf{x}$ and t. The Navier-Stokes equations governing the fluid flow, in conservation form, are

$$\frac{\partial \rho}{\partial t} + \nabla \cdot (\rho \mathbf{u}) = 0 \quad \text{in } \Omega \text{ for } (0,T), \tag{1}$$

$$\frac{\partial (\rho \mathbf{u})}{\partial t} \tag{2}$$

$$\frac{\partial (\rho e)}{\partial t} + \nabla \cdot (\rho e \mathbf{u}) + \nabla \cdot (p\mathbf{u}) - \nabla \cdot (\mathbf{T}\mathbf{u}) + \nabla \cdot \mathbf{q} = 0 \quad \text{in } \Omega \text{ for } (0,T) \tag{3}$$

Here ρ, $\mathbf{u}$, p, $\mathbf{T}$, e, and $\mathbf{q}$ are the density, velocity, pressure, viscou_ stress tensor, the total energy per unit mass, and the heat flux vector, respectively. The viscous stress tensor is defined as $\mathbf{T} = \mu((\nabla \mathbf{u}) + (\nabla \mathbf{u})^T) + \lambda(\nabla \cdot \mathbf{u})\mathbf{I}$, where μ and λ are the viscosity coefficients. It is assumed that $\lambda = -(2/3)\mu$. For ideal gases, the equation of state is $p = (\gamma - 1)\rho i$, where γ is the ratio of specific heats and i is the internal energy per unit mass that is related to the total energy per unit mass and velocity as $i = e - (1/2)\|\mathbf{u}\|^2$. The heat flux vector is defined as $\mathbf{q} = -\kappa \nabla \theta$, where κ is the heat conductivity and θ is the temperature. The temperature and internal energy are related as $\theta = (\gamma - 1/R)i$, where R is the ideal gas constant. Prandtl number (P_r), assumed to be specified, relates the heat conductivity to the fluid viscosity. It is defined as $P_r = (\gamma R/\mu)(\gamma - 1)\kappa$.

The compressible Navier-Stokes Equations (1), (2), and (3) can be written in the conservation variables

$$\frac{\partial \mathbf{U}}{\partial t} + \frac{\partial \mathbf{F}_i}{\partial x_i} - \frac{\partial \mathbf{E}_i}{\partial x_i} = \mathbf{0} \quad \text{in } \Omega \text{ for } (0,T), \tag{4}$$

where $\mathbf{U} = (\rho, \rho u_1, \rho u_2, \rho e)^T$, is the vector of conservation variables, and $\mathbf{F}_i$ and $\mathbf{E}_i$ are, respectively, the Euler and viscous flux vectors defined as

$$\mathbf{F}_i = \begin{pmatrix} u_i \rho \\ u_i \rho u_1 + \delta_{i1} p \\ u_i \rho u_2 + \delta_{i2} p \\ u_i(\rho e + p) \end{pmatrix} \qquad \mathbf{E}_i = \begin{matrix} 0 \\ \tau_{i1} \\ \tau_{i2} \\ -q_i + \tau_{ik} u_k \end{matrix} \tag{5}$$

Here u_i, q_i, and τ_{ik} are the components of the velocity, heat flux, and viscous stress tensor, respectively. In the quasi-linear form, Eq. (4) is written as

$$\frac{\partial \mathbf{U}}{\partial t} + \mathbf{A}_i \frac{\partial \mathbf{U}}{\partial x_i} - \frac{\partial}{\partial x_i}\Big(\qquad \text{in } \Omega \text{ for } (0,T), \tag{6}$$

where $\mathbf{A}_i = (\partial \mathbf{F}_i / \partial \mathbf{U})$ is the Euler Jacobian Matrix, and $\mathbf{K}_{ij}$ is the diffusivity matrix satisfying the relationship $\mathbf{K}_{ij}(\partial \mathbf{U}/\partial x_j) = \mathbf{E}_i$. Corresponding to Eq. (6), the following boundary and initial conditions are chosen

$$\mathbf{U} = \mathbf{g} \quad \text{in } \Gamma_g \text{ for } (0,T), \tag{7}$$

$$\mathbf{n} \cdot \mathbf{E} = \mathbf{h} \quad \text{in } \Gamma_h \text{ for } (0,T), \tag{8}$$

$$\mathbf{U}(\mathbf{x}, 0) = \mathbf{U}_0 \quad \text{in } \Omega \tag{9}$$

$$+\sum_{e=1}^{n_{el}}\int_{\Omega^e}\delta\left(\frac{\partial \mathbf{W}^h_{n+1}}{\partial x_i}\right)\cdot\left(\frac{\partial \mathbf{U}^h}{\partial x_i}\right)d\Omega = \int_{\Gamma_h}\mathbf{W}^h_{n+1}\cdot\mathbf{h}^h d\Gamma \qquad (11)$$

In the variational formulation given by Eq. (11), n_{el} is the number of elements and Ω^e, $e=1, 2, \ldots, n_{el}$, are the finite element subdomains. The first two terms and the right-hand-side constitute the Galerkin formulation of the problem. The first series of element-level integrals in Eq. (11) are the SUPG stabilization terms added to the variational formulation to stabilize the computations against node-to-node oscillations in the advection-dominated range. The second series of element level integrals in the formulation are the shock capturing terms that stabilize the computations in the presence of sharp gradients. The stabilization coefficients δ and τ are the ones that are used by Mittal [11, 12] and quite similar to those employed by Aliabadi and Tezduyar [18]. All the flows, presented in this article, are computed using equal-in-order linear elements.

The time discretization of the variational formulation given by Eq. (11) is done *via* the generalized trapezoidal rule. For unsteady computations we choose the parameter value to yield second-order accuracy in time.

4. RESULTS AND DISCUSSIONS

All the computations reported in this article are carried out in 64 bit precision using linear triangular elements. Many of the flow problems have been computed using *EDICT* on the shared-memory parallel computers of the SGI multiple-processor systems (*Origin*-200). The non-linear equation systems resulting from the finite-element discretization of the flow equations are solved using the Generalized Minimal RESidual *GMRES* technique [19] in conjunction with block-diagonal preconditioners. For all the cases, unless mentioned otherwise, the viscosity and thermal conductivity coefficients are constant. The Prandtl Number is 0.72 and the ratio of specific heats, γ, is 1.4.

4.1. $M=2$, $Re=1000$ Flow Past a Circular Cylinder

The base mesh, employed for this flow problem, consists of 8452 triangular elements and 4396 nodes. The Reynolds number, based on the diameter of the cylinder and the free-stream values of the velocity and kinematic viscosity, is 1000. The cylinder wall is assumed to be adiabatic and the no-slip condition is specified for the velocity on the surface of the cylinder. All the variables are specified on the upstream boundary. At the downstream boundary, we specify a Neumann type boundary condition for the velocity and energy that correspond to zero viscous stress and heat flux vectors. The computations are initiated with free-stream conditions in the entire domain and continue till the steady-state norm of the solution falls below a certain desired value. The elements in Mesh-1 that need enhanced discretization, as reported by the error-indicator, are subdivided into sixteen elements. Figure 1 shows the Level-2 mesh and the density field for the steady-state solution. The numbers of elements and nodes in the mesh are denoted by *ne* and *nn*, respectively. One can observe a strong bow shock upstream of the cylinder and a weaker tail shock in the wake. The shock stand-off distance compares quite well with experimental observations [20]. It can also be observed that the shock has been captured quite well within two to three elements of the refined mesh. The Level-2 refinement is mostly in the region of shocks and boundary layer.

4.2. $M=3$, $Re=16,800$ Flow Past a Compression Corner

In this problem Mach 3 flow passes over a flat plate and then a compression corner of 10°. This is one of the test cases studied by Carter [15] and the flow conditions are identical to the ones described by him. The computational domain covers the

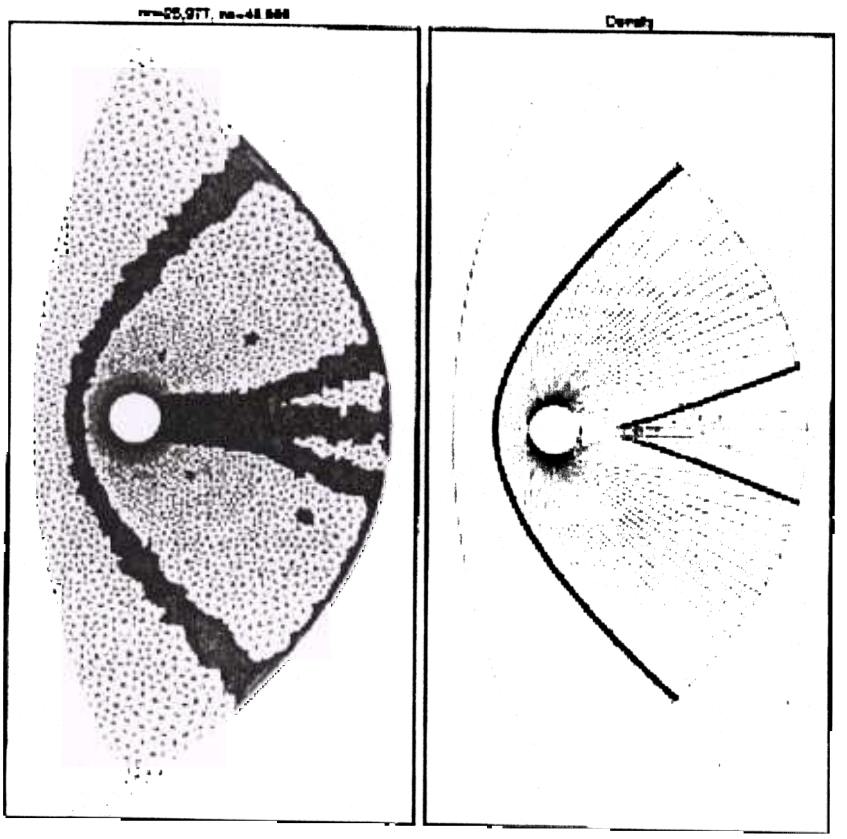

FIGURE 1 $Re = 1000$, $M = 2$ flow past a cylinder: the *Level*-2 mesh and the density field for the steady-state solution. The base mesh consists of 4396 nodes and 8452 triangular elements.

area $-0.2 \leq x \leq 1.8$, $0 \leq y \leq 0.575$ on the plate and a height of 0.575 above the wall past the corner. The flat plate is placed $x = 0$ and the 10° corner at $x = 1.0$. At the inflow and top boundary all flow variables are specified. On the solid surface (plate and the compression ramp) no-slip condition is specified on the velocity while the wall temperature is prescribed as the stagnation temperature of the free-stream flow. Symmetry conditions are specified on the line of symmetry for $x < 0$, $y = 0$ while no conditions are specified on the outflow boundary. The Reynolds number based on the distance between the leading edge of the plate and compression corner is 16,800. The dependence of the viscosity on the temperature is modeled *via* the Sutherland's law of viscosity. A mesh with 5386 nodes and 10520 triangular elements is utilized to compute the solution. Once the steady-state solution is realized it is used to compute the solution on the *Level*-2 mesh. Figure 2 shows the mesh for the *Level*-2 computations and the steady-state mach number, pressure, density and temperature fields. The leading-edge shock due to the development of boundary layer on the flat plate has been captured quite well. The separation of the flow ahead of the corner and its subsequent re-attachment downstream of the corner results in a region of recirculation which can be observed in the solution. The error indicator picks up the regions in the flows that involve shocks and shear layer and the corresponding elements are refined to improve the accuracy of the computation. The solution obtained with the base mesh (Level-0) shows a similar behavior except that the solution with Level-2 mesh has crisper shocks. The separation point of the flow for the present calculations is at $x = 0.89$. Shakib [14], Hung and MacCormack [16] and Carter [15] have reported this value to be 0.88, 0.89 and 0.84, respectively, for their computations.

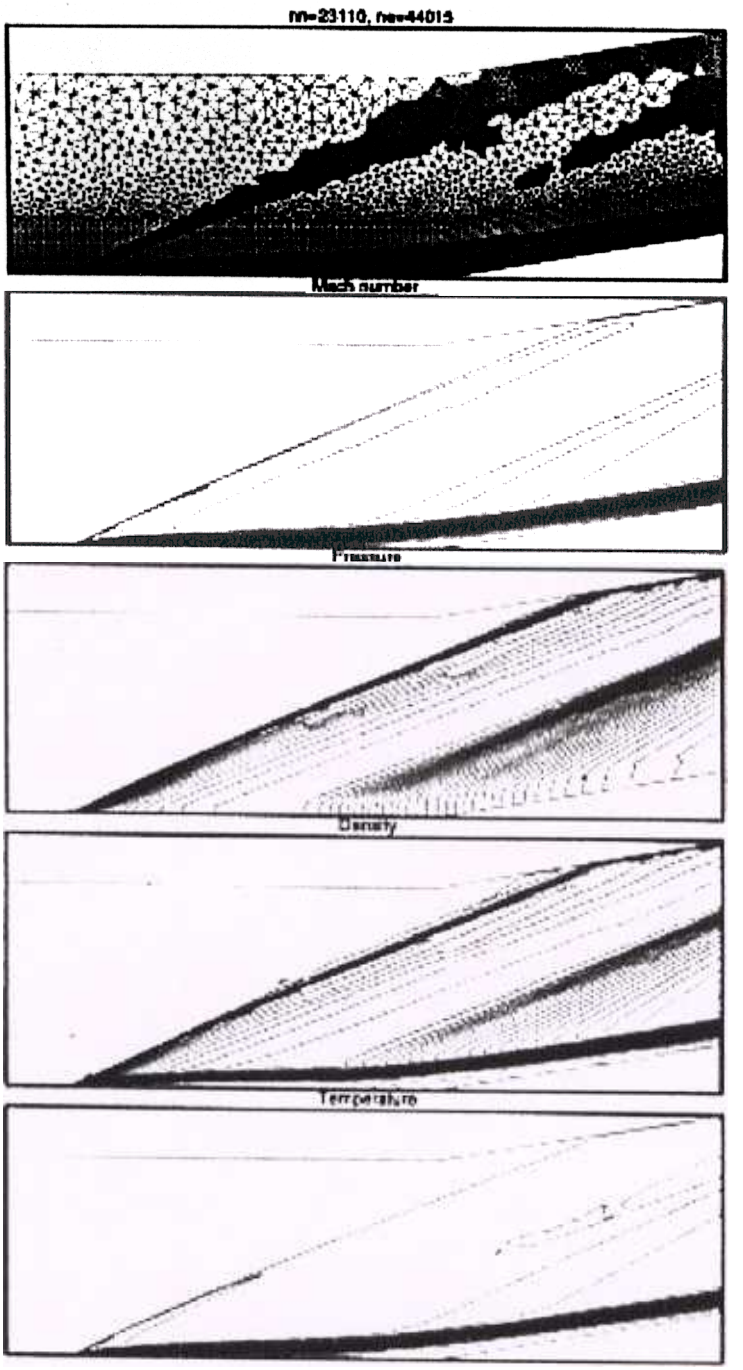

FIGURE 2 $Re = 16{,}800$, $M = 3$ flow over a compression corner: the *Level*-2 mesh and the computed flow field for the steady-state solution.

It is interesting to contrast this solution to that for the inviscid flow case. In the absence of viscosity, there will be no boundary layer and one would expect an oblique shock at the compression corner. In the present case, due to viscous effects, the oblique shock is replaced by a compression fan. Figure 3 shows the variation of the pressure and the skin friction coefficients on the solid surface. It can be observed that the curves obtained with the Level-0 and Level-2 meshes are almost identical.

solution very rapidly. The location of the shocks and flow separation are predicted quite well by the present formulation. This establishes our confidence in the formulation and its implementation for computing internal flows.

4.4. $M=5$ Flow in a Supersonic Diffuser

The method is used to analyze the flow through a diffuser section in a supersonic wind-tunnel. The schematic of the computational domain is shown in Figure 7. Supersonic inflow conditions are assumed at the inlet of the test-section. The diffuser section consists of a converging section followed by a constant-area section. The flow slows down in the diffuser *via* a train of oblique shocks and viscous diffusion. Sometimes, the diffuser section ends with a diverging section to slow the subsonic flow even further. This has not been modeled in the present simulations. The diffuser walls are assumed to be at reservoir temperature and the no-slip condition is specified for the velocity. At the downstream boundary, Neumann type boundary conditions for the velocity and energy are specified that correspond to zero viscous stress and heat flux vectors. In case a significant part of the flow at the exit becomes subsonic, the outflow conditions need a modification. In Figure 7, the half-height of the test-section is A_1 while that of the constant-area section of the diffuser is A_2. The test section length is L_t and the length of the constant-area section is L_c. The angle of the converging part is θ. The Reynolds number is defined as $Re=(a_0 A_t \rho_0/\mu)$ where, a_0, ρ_0 and μ are, respectively, the speed of sound, density and viscosity for reservoir conditions and A_t is the half-height at the nozzle throat. The throat and reservoir conditions are calculated by assuming an isentropic flow between the reservoir and test-section inlet.

Shown in Figure 8 is the solution for the flow through a diffuser with $A_2/A_1=0.775$, $L_t=2.0$, $L_c=6.0$ and $\theta=10°$. The Reynolds number is 1.5×10^5 and inlet Mach number is 5. The figure shows the Level-0 finite element mesh and the Mach number field at various time instants as the flow reaches a steady-state. The mesh is symmetric about the tunnel center-line and the entire computations are carried out with a *Level*-0 mesh. The computations are initiated with the fluid at rest in the tunnel. A set of weak oblique shocks are formed right at the inlet because of the presence of boundary layer at the tunnel wall. These shocks are not present in a real tunnel. This discrepancy can be avoided by either specifying an appropriate boundary layer flow at the inlet or by simulating the entire tunnel. Another set of oblique shocks are formed at the wedge corresponding to the inlet of the diffuser section. These shocks are reflected from the diffuser walls and alternate regions of compression and expansion of flow can be observed. The interaction of the boundary layer with the alternate regions of compression and expansion leads to its undulating thickness. In regions just downstream of the shocks, the boundary layer thickens and sometimes separates due to the adverse pressure gradient. The thickening of the boundary layer increases the shock strength further. This non-linear coupling is further complicated by the unsteady effects during the development of the

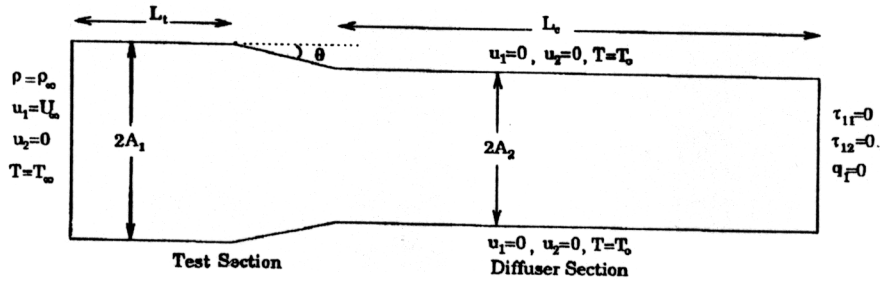

FIGURE 7 Flow in a supersonic diffuser: problem description

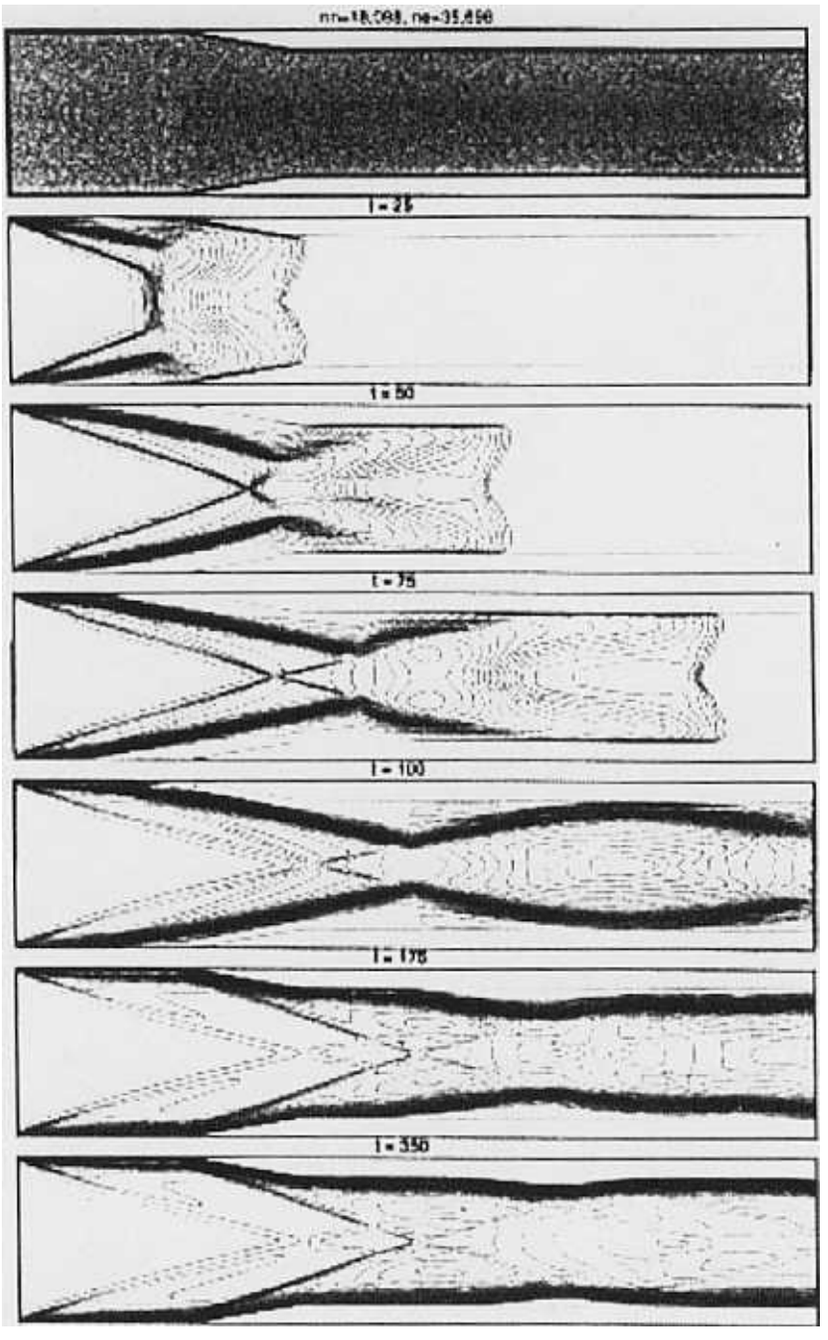

FIGURE 8 $M = 5$, $Re = 1.5 \times 10^5$ flow in a supersonic diffuser with $A_2/A_1 = 0.775$, $L_t = 2.0$, $L_c = 6.0$: the mesh and the mach number field for the computed solution at various times.

flow. For the steady-state solution, the pressure recovery is quite poor for this diffuser. The exit Mach number at the tunnel center-line is, approximately, 4.6 which is quite high.

Figure 10 shows the steady-state solution for a similar diffuser with a larger length of the constant-area section ($L_c = 16.7$). This solution has been computed with the Level-2 mesh and as can be noticed the oblique shock train and its interaction with the boundary layer has been captured in greater detail. The pressure recovery in the present case is slightly higher than that in the previous case

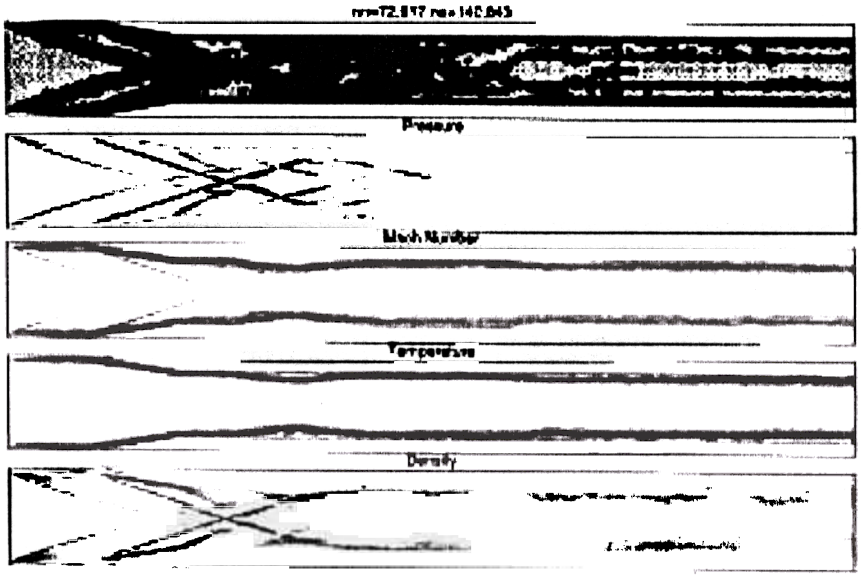

FIGURE 9 $M=5$, $Re=1.5\times10^5$ flow in a supersonic diffuser with $A_2/A_1=0.775$, $L_t=2.0$, $L_c=16.7$: the *Level*−2 mesh, flow pictures for the steady-state solution.

pointing to the significance of viscous diffusion in supersonic diffusers. The exit Mach number at the center-line is, approximately, 3.7 which is still fairly high.

It is well known that for a fixed geometry diffuser the value chosen for A_2/A_1 must not be less than that required to *start* the flow. Otherwise, an unsteady shock-wave, such as the one obtained during start-up, is not swallowed by the diffuser and the tunnel may *unstart*. This simulation is an effort to understand the dynamics of the unsteady shock interactions that cause this phenomenon. A fully developed *Mach* 5 flow is assumed at the inlet of the test-section ($L_t=2.0$) of a wind-tunnel with a diffuser section corresponding to $A_2/A_1=0.3$, $L_c=6.0$ and $\theta=7.5°$. The computations are initiated with fluid at rest in the tunnel. With such a narrow constant-area section of the diffuser it is expected that the start-up shock will not pass through and should *unstart* the tunnel. Figure 10 shows the solution to this flow problem at various time instants. It can be observed from the figure that initially a set of oblique shocks form at the test-section inlet due to boundary layer and at the wedges of the converging part of the diffuser section. Very soon the oblique shock pattern looses its symmetry and it is seen that the shock angle for the one on the upper wall increases while that for the lower wall decreases. The flow in the constant-area section of the diffuser also becomes unsymmetric and an interesting unsteady interaction between the boundary layer and shock waves takes place. Later, the oblique shock on the upper wall of the tunnel increases in strength and moves upstream. The shock on the lower wall becomes weaker and later disappears while the one on the upper wall takes the form of a normal shock. The normal shock moves upstream and the computations breakdown when it reaches the inlet of the test-section. In a real set-up, the shock will go further upstream into the nozzle block and stall the tunnel.

4.5. Flow in a Supersonic Wind-tunnel

Figure 11 shows a typical wind-tunnel that is simulated in the present work. It also indicates the boundary conditions used in the computations. At the upstream boundary the stagnation pressure (p_o) and total enthalpy (h_o) are specified along with the direction of the flow (along the x-axis). The flow velocity at the inlet is unknown and so is the density. It is assumed that the flow between the

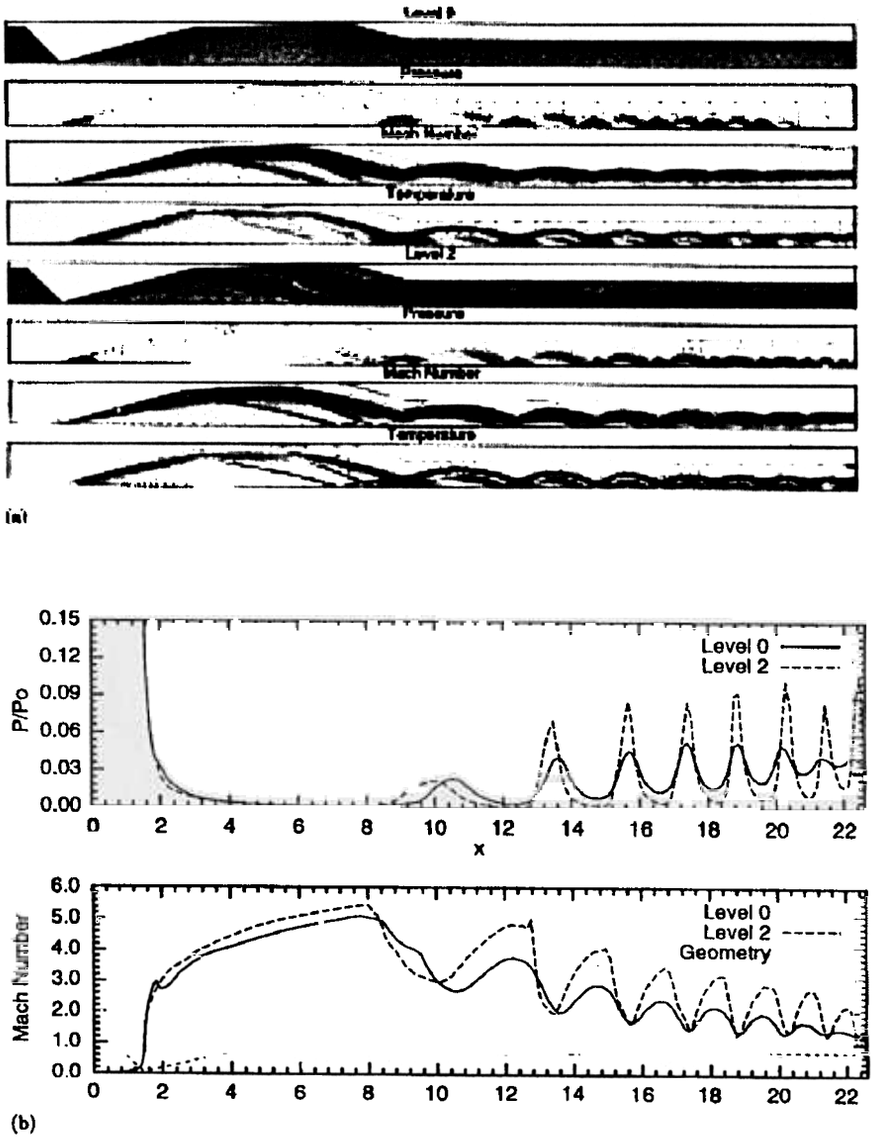

FIGURE 12 $Re = 4 \times 10^5$ flow in a supersonic tunnel with a wedge nozzle block and $A_1/A_t = 25$, $A_2/A_1 = 0.7$, $L_t = 4.0$, $L_c = 12.0$, $p_o/p_e = 25$: the steady-state solution. (a) The finite element mesh, pressure, mach number and the density fields for the *Level 0* (6902 nodes and 13,098 elements) and *Level 2* (48,203 nodes and 92,433 elements) solutions, respectively. (b) Variation of pressure and mach number along the tunnel center-line.

reservoir and upstream boundary is isentropic and this condition is used to relate the density and pressure at the upstream boundary to the ones at reservoir (stagnation values). The walls of the tunnel are assumed to be maintained at the stagnation temperature and the velocity satisfies the no-slip condition. At the tunnel exit, a pressure value is specified and the viscous stress vector is assigned a zero value. To save on the computational expenses, only one half of the tunnel is simulated and symmetry conditions are imposed along the tunnel center-line: the vertical component of the velocity is set to zero and so are the viscous and heat flux vectors. The computations